

Experimental assessment of a Micro-Pulse Lidar system in comparison with reference lidar measurements for aerosol optical properties retrieval

5 Carmen Córdoba-Jabonero^{1*}, Albert Ansmann², Cristofer Jiménez², Holger Baars²,
María-Ángeles López-Cayuela¹, and Ronny Engelmann²

¹Instituto Nacional de Técnica Aeroespacial (INTA), Atmospheric Research and Instrumentation Branch, Torrejón de Ardoz, 28850-Madrid, Spain

²Leibniz Institute for Tropospheric Research (TROPOS), Leipzig, Germany

Correspondence to: Carmen Córdoba-Jabonero (cordobajc@inta.es)

10 **Abstract.** Simultaneous observations of a polarized Micro-Pulse Lidar (P-MPL) system and two reference
European Aerosol Research Lidar Network lidars, running at the Leipzig site (Germany, 51.4°N 12.4°E,
125 m a.s.l.), were performed during a comprehensive two-month field intercomparison campaign in
summer 2019. An experimental assessment regarding both the overlap (OVP) correction of the P-MPL
15 signal profiles and the volume linear depolarization ratio (VLDR) analysis, together with its impact in the
retrieval of the aerosol optical properties, is achieved, describing also the experimental procedure used. The
optimal lidar-specific OVP function is experimentally determined, highlighting that the one delivered by
the P-MPL manufacturer cannot be long used. Among the OVP functions examined, the averaged one
between those obtained from the comparison of the P-MPL observations with those of the other two
reference lidars seems to be the best proxy at both near- and far-field ranges. In addition, the impact of the
20 OVP function in the accuracy of the retrieved profiles of the total particle backscatter coefficient (PBC)
and the particle linear depolarization ratio (PLDR) is examined. The VLDR profile is obtained and
compared to that derived from the reference lidar, showing it needs to be corrected by a small offset value
within a good accuracy. Once P-MPL measurements are optimally (OVP, VLDR) corrected, both the PBC
and PLDR profiles can be accurately derived, being in good agreement with reference aerosol retrievals. In
25 overall, as a systematic requirement for lidar systems, an adequate OVP function determination and VLDR
testing analysis is needed to be performed in a regular basis to correct the P-MPL measurements in order
to derive suitable aerosol products. A dust event as observed at Leipzig in June 2019 is used for illustration.

1 Introduction

30 Active remote sensing is an excellent tool for vertical monitoring of the atmosphere. In particular, aerosol
lidar systems have demonstrated to be a suitable instrumentation for aerosol and cloud profiling in both the
troposphere and stratosphere (e.g., Amiridis et al., 2015; Baars et al., 2019). Tropospheric aerosols are
usually confined up to 7-8 km height under aerosol intrusion conditions (e.g., Mattis et al., 2008; Pappalardo
et al., 2013); otherwise, they are mostly concentrated in the ABL (around less than 1.5 km height). Indeed,
lidar systems are widely used due to their high vertical spatial and temporal resolution.

35 Ground-based lidar networks are widely operative within the GAW (Global Atmospheric Watch) Aerosol
Lidar Observations Network (GALION); among them, there are those extended at continental scales, as

EARLINET (European AeRosol Lidar NETwork, www.earlinet.org; Pappalardo et al., 2014), which belongs also to the Aerosol Cloud and Trace Gases Research Infrastructure (ACTRIS, www.actris.eu), AD-NET (Asian Dust and aerosol lidar observation network, www-lidar.nies.go.jp/AD-Net; Sugimoto et al., 2008), and LALINET (a.k.a. ALINE, Latin American Lidar NETwork, www.lalinet.org; Barbosa et al., 2014). In addition, there are other aerosol networks like MPLNET (Micro-Pulse Lidar NETwork, mplnet.gsfc.nasa.gov; Welton et al., 2001), within GAW/GALION, and PollyNET (PORTabLe Lidar sYstem NETwork, <http://polly.tropos.de>; Baars et al., 2016), operated as a part of EARLINET, whose sites are distributed around the world.

The use of the lidar observations with polarization capabilities is increasing as the lidar depolarization measurements allow a better aerosol speciation (dust, marine aerosol, anthropogenic pollution, volcanic ash, biomass burning, pollen, ...) as well as the separation of the optical properties (backscatter, extinction) of particle components within complex aerosol mixtures with vertical resolution (i.e., Ansmann et al., 2011; Burton et al., 2014; Yu et al., 2015; Córdoba-Jabonero et al., 2018; Bohlmann et al., 2019). Therefore, new and promising methods based on the particle depolarization ratio were developed and used to derive aerosol profiles in terms of particle mass concentration, separately for the coarse and fine modes (i.e., Mamouri and Ansmann, 2017), in addition to estimate both the cloud-condensation nuclei (CCN) and ice-nucleating particle (INP) concentrations (i.e., Mamouri and Ansmann, 2016).

The atmospheric lidar scanning provides an accurate characterization at all ranges; however, lidar systems present an incomplete response in the near-range observational field due to the partial intersection of the field-of-view between the transmitter and the receiver for both the biaxial and coaxial lidar configurations. Therefore, lidar signal profiles must be corrected by this near-field loss of signal, that is, the overlap (OVP) correction (Wandinger and Ansmann, 2002). The full-OVP height depends on the lidar system (e.g., Wandinger et al., 2016).

During the last two decades, Micro-Pulse Lidar (MPL) systems (Campbell et al., 2002; Welton et al., 2002; manufacturer: Sigma Space Corp., currently Droplet Measurement Technologies) were deployed at different latitudes and many of them in the frame of MPLNET; since few years a polarized MPL version (P-MPL) is the standard lidar system in this network. Both MPL and P-MPL observations have been widely performed for continuous monitoring of aerosols and clouds. In particular, MPL/P-MPL measurements were used for: Atmospheric Boundary Layer (ABL) height retrievals (Lewis et al., 2013; Toledo et al., 2014, 2017), detection and characterization of both cirrus clouds (Campbell et al., 2016; Lewis et al., 2016; Córdoba-Jabonero et al., 2017; Lolli et al., 2017; Campbell et al., 2021) and Polar Stratospheric Clouds (PSC) (Campbell et al., 2008; Córdoba-Jabonero et al., 2013), depolarization-based characterization of the optical properties of different aerosol mixtures (Sicard et al., 2016; Córdoba-Jabonero et al., 2016, 2018), aerosol mass concentration estimation either in synergy with airborne measurements (Córdoba-Jabonero et al., 2016) or in comparison with forecast model simulations (Córdoba-Jabonero et al., 2019), determination of the precipitation intensity (Lolli et al., 2018; Lolli et al., 2020) and the cloud thermodynamic phase (Lewis et al., 2020) and assessment of the radiative effect of aerosols and cirrus clouds (Campbell et al., 2016; Lolli et al., 2017; Córdoba-Jabonero et al., 2020, 2021; Campbell et al., 2021; Sicard et al., 2021), among others. Those works have demonstrated a good MPL performance in aerosol/cloud research. The P-MPL is an elastic coaxial single-wavelength (532 nm) system and, differing from older MPL versions

(Campbell et al., 2002; Welton et al., 2002), incorporates depolarization capabilities (Flynn et al., 2007). As a value-added improvement, it can operate in routine continuous (24/7) mode. However, the P-MPL system needs to be well characterized in terms of the backscattered lidar signal detected by both
80 depolarization channels of the instrument (Flynn et al., 2007; Welton et al., 2018) in order to retrieve plausible aerosol optical properties. In particular, due to the very narrow telescope field of view, the lidar system is reaching the full-OVP height at relatively high altitudes (typically at 4-6 km height; Campbell et al., 2002), being particularly relevant for tropospheric aerosol research. For this reason, an accurate overlap correction, among other features, is needed for MPL systems.

85 MPLNET have established methods for overlap calibration, as those described in Berkoff et al. (2003). They are based on either performing measurements under atmospheric stable and homogeneous conditions with the MPL pointing in horizontal, or making use of a secondary wide field-of-view receiver (WFR) telescope. However, both of them could not be yet applied on site to the MPL system examined in this study. Hence, an alternative experimental procedure for the OVP function determination is introduced in this work, which
90 is based on the cross-comparison of the backscattered signal recorded by the uncorrected lidar system (our MPL) with respect to that collected by a reference (overlap-corrected) lidar. A similar methodology has been also used for the overlap correction of other lidars and ceilometers (i.e., Guerrero-Rascado et al., 2010; Sicard et al., 2020; and references therein). In this framework, an experimental campaign was planned at the EARLINET Leipzig site (Germany), and, in particular, devoted to simultaneously compare the
95 observations of a P-MPL system with reference well-calibrated lidar measurements in order to determine the required P-MPL performance.

The aim of this work is threefold: 1) to achieve an OVP correction of a P-MPL system, i.e., to estimate the experimental OVP function for correcting the P-MPL measurements; 2) to evaluate the volume linear depolarization ratio (VLDR), which is a lidar-derived parameter independent of OVP correction; and 3) to
100 determine the P-MPL correction-induced effects on the retrieval of optical properties, both the height-resolved particle backscatter coefficient (PBC) and particle linear depolarization ratio (PLDR). **Section 2** introduces the methodology for that purpose: an overview of the field intercomparison campaign performed, a brief description of both the P-MPL and reference lidar systems used, and the experimental approaches applied for the data analysis, regarding the experimental estimation of the OVP function of the
105 P-MPL system (error processing is described in **Annex A**), the evaluation of the VLDR, and the retrieval of the particle optical properties. Results are presented in **Section 3**. A dust case as observed during the field campaign is used for that purpose. Main conclusions are presented in **Section 4**.

2 Methodology

2.1 Field campaign overview

110 During a field campaign carried out at the EARLINET station of Leipzig, Germany (51.35°N 12.43°E, 125 m a.s.l.), managed by the Leibniz Institute for Tropospheric Research (TROPOS), for 6 weeks in June-July 2019, the performance of a P-MPL system was experimentally examined, with a special emphasis on the OVP correction and VLDR evaluation. The lidar system used was the MPL44245 unit (formerly Sigma Space Corp., currently Droplet Measurement Technologies) routinely operating at the MPLNET/El

115 Arenosillo station (https://mplnet.gsfc.nasa.gov/data_all&s=El_Arenosillo), sited at Huelva, Spain
 (ARN/Huelva, 37.1°N 6.7°W, 40 m a.s.l.), which is managed by the Spanish Institute for Aerospace
 Technology (INTA). Both stations are also AERONET (AErosol RObotic NETwork,
<aeronet.gsfc.nasa.gov>) sites, accomplishing the requisite for co-location of both networks for the elastic
 retrieval of the aerosol optical properties. For the campaign, this P-MPL was temporarily deployed outside
 120 MPLNET at Leipzig to be compared against two EARLINET lidars routinely operative in this station, as
 Polly (POrtabLe Lidar sYstem; Althausen et al, 2009; Engelmann et al., 2016) and MARTHA
 (Multiwavelength Tropospheric Raman lidar for Temperature, Humidity, and Aerosol profiling; Jiménez
 et al., 2018) systems. They were used as reference because these lidars are well characterized with respect
 to EARLINET quality assurance standards (e.g., Böckmann et al., 2004; Pappalardo et al., 2004;
 125 Freudenthaler et al., 2008; Pappalardo et al., 2014; Wandinger et al., 2016; Belegante et al., 2016; Bravo-
 Aranda et al., 2016; Freudenthaler et al., 2016).

2.2 Lidar systems

2.2.1 Polarized Micro-Pulse Lidar (P-MPL)

The P-MPL system (Sigma Space Corp./Droplet Measurement Technologies, v. MPL-4B) is the standard
 130 lidar currently operating within MPLNET. It is an elastic lidar in coaxial configuration with depolarization
 capabilities operating in full-time (24/7) mode. Among the principal optical features, the Nd:YVO₄ laser
 emission at 532 nm, with a pulse energy of 6-8 μ J and a repetition rate of 2500 Hz, is recorded by a unique
 avalanche photodiode detector (APD), and the receiver system presents a field-of-view (FOV) of 80 μ rad
 full angle and the telescope diameter is 18 cm wide (Sigma Space Corp., MPL system information
 135 handbook, 2018). P-MPL vertical profiles are routinely acquired with 1-min integrating time and 15-m
 vertical resolution (in particular, for the ARN/Huelva P-MPL system) up to 30 km height. Main
 instrumental features of the P-MPL system are shown in **Table 1**.

Table 1: Main instrumental features of the lidar systems.

Lidar system	P-MPL	Polly	MARTHA
Routine operation	24/7	24/7	Supervised
Lidar Networks	MPLNET	EARLINET	EARLINET
Transmitter properties			
Wavelength (nm)	532	532 (*)	532 (*)
Energy/pulse (mJ)	0.006-0.008	400	1000
Pulse frequency (Hz)	2500	20	30
Eye-safety	Yes (ANSI Class II)	No	No
Receiver properties			
Telescope diameter (cm)	18	30	80
Telescope focal length (m)	2.23	0.89	9
FOV (μ rad full angle)	80.4	1000	500
Depolarization	Yes	Yes	Yes
Raman detection	No	Yes	Yes

140 (*) Used in this study.

The optical layout of the MPL-4B version is schematically shown in Flynn et al. (2007; see their Fig. 1). The laser light is alternatively transmitted linearly and circularly polarized to the atmosphere by switching between two retardation modes of a ferroelectric liquid crystal (FLC) rotator. The corresponding backscattered light to those two polarized states by passing through a beam splitter to the single APD is recorded in dependence of the polarizing or depolarizing atmospheric particles leading to the suppression or not, respectively, of the orthogonally-detected signal w.r.t. the transmitted one into the single APD. Those two polarized signals are semi-simultaneously detected by alternatively switching in the basis of 50%/50% the FLC polarization mode within every integrating minute. Note that the P-MPL pulse frequency is 2500 Hz, and the polarization state is switched every 250 pulses, but just 249 pulses are collected since one of the pulses is discarded during the FLC switching time ($\sim 100 \mu\text{s}$). That is, those two signals are alternatively detected by the same APD, being recorded in two polarized channels, i.e., the 532-nm cross-signal (P_{cross}) and the 532-nm co-signal (P_{co}) (see a more detailed description in Flynn et al., 2007). Therefore, since no potentially existing efficiency or alignment differences are between those two signal-channels (as used a single APD), no corrections for these effects are required, as it is typically needed for ordinary two-channel polarization lidars. Particular regular calibrations and signal processing were applied, which are the same as those described by Campbell et al. (2002) and Welton et al. (2002), and also by Flynn et al. (2007), whose data processing techniques remain also applicable for P-MPL systems, as indicated by Welton et al. (2018). Therefore, the measured lidar signal in those two polarized-channels is used to derive both the P-MPL total range-corrected signal (RCS), P^{MPL} , and the volume linear depolarization ratio (VLDR), δ^V , by adapting the methodology as described in Flynn et al. (2007), that is,

$$P^{MPL} = P_{co} + 2 P_{cross}, \text{ and} \quad (1)$$

$$\delta^V = \frac{P_{cross}}{P_{co} + P_{cross}}. \quad (2)$$

This data processing has been successfully applicable in particular studies (e.g., Sicard et al., 2016; Córdoba-Jabonero et al., 2018; Lewis et al., 2020), independently of that established in MPLNET. Among the required routine instrumental P-MPL corrections (Campbell et al., 2002; Welton et al., 2002), the OVP is a concerning issue, since the typical full-OVP height is reached at rather high altitudes (usually at 4-5 km height), affecting thus the aerosol profiles at ranges in the overall boundary layer and part of the troposphere. Hence, an important issue to be achieved is the particular overlap correction function for this particular P-MPL system. After sale, the P-MPL system is delivered with an original OVP function as provided by the manufacturer company (formerly Sigma Space Corp., currently Droplet Measurement Technologies), which, however, must be re-evaluated with time. Indeed, one of the goals of this work is to show the experimental procedure, similar to other usually applied (i.e., Guerrero-Rascado et al., 2010; Sicard et al., 2020), to obtain a new OVP function for the P-MPL lidar as compared to the original one (see later Sect. 2.3.1) together to examine its effects in the retrieval of the optical properties.

2.2.2 POrtabLe Lidar sYstem (Polly)

The EARLINET Polly (POrtabLe Lidar sYstem) lidars are sophisticated, automated Raman-polarization lidar systems for scientific purpose, but with the advantage of an easy-to-use and well-characterized

instrument with same design, same automated operation, and same centralized data processing delivering
 180 near-real-time data products. Polly systems have been developed and constructed at TROPOS with
 international partners since 2002 (Engelmann et al., 2016). All Polly lidar systems are designed for
 automatic and unattended operation in 24/7 mode. Meanwhile 12 Polly lidar systems are distributed around
 the globe (e.g., Baars et al., 2016). The Polly lidar system used as a reference in this comparison analysis,
 is the first one of the Polly family (Engelmann et al., 2016), which was substantially upgraded in 2016 (v.
 185 Polly_1v2). It emits linearly polarized light at 532 nm with 5 receiver channels: the elastically backscattered
 light at 532 nm, the cross-polarized light at 532 nm, the co-polarized light at 532 nm, the rotational-Raman
 scattered light near 532 nm, and the vibrational-rotational Raman scattered light at 607 nm. Its full-OVP is
 reached at around 300-500 m height, and thus preferred for the P-MPL OVP correction purpose. Profiles
 of the Polly range-corrected signal, P^{Polly} , are routinely derived by using sample settings with 7.5-m
 190 vertical resolution and 30-sec temporal integration. The main instrumental features of the Polly system are
 shown in **Table 1**.

2.2.3 Multiwavelength Atmospheric Raman lidar for Temperature, Humidity, and Aerosol profiling (MARTHA)

The second EARLINET lidar, which is used as a reference in this work, is the dual receiver field-of-view
 195 (RFOV) Multiwavelength polarization/Raman lidar for Temperature, Humidity, and Aerosol profiling
 (MARTHA) (Mattis et al., 2008; Schmidt et al., 2013, Jimenez et al., 2019). MARTHA has a powerful
 laser, transmitting in total 1 J per pulse at a repetition rate of 30 Hz, with an 80-cm telescope diameter,
 being thus well designed for tropospheric and stratospheric aerosol observations. This lidar system
 measures Raman signals at 532 nm (P^{MARTHA} , which is that used in this work) and 607 nm and the
 200 polarization-sensitive 532-nm backscatter signals at two RFOVs so that, besides aerosol profiles, cloud
 microphysical properties can be retrieved from measured cloud multiple scattering effects. MARTHA can
 provide the 532-nm particle depolarization ratio as measured with the smaller RFOV, and also the 355-,
 532-, and 1064-nm particle backscatter coefficients and the 355- and 532-nm extinction coefficient profiles
 with their corresponding lidar ratio profiles. For this large telescope (and a selected receiver FOV of 0.5
 205 mrad) the overlap between laser beam and receiver FOV is complete around 2000 m height. The overlap
 profile of this laboratory lidar is very stable. The main instrumental features of the MARTHA system are
 shown in **Table 1**.

2.3 Experimental estimation of the overlap (OVP) function

The overlap (OVP) function, F_{OVP} , is used to correct the P-MPL (no OVP-corrected) RCS profiles,
 210 $P^{MPL}(z)$, as obtained from **Eq. 1**, at near-field altitudes, that is,

$$P_{OVP}^{MPL}(z) = P^{MPL}(z) / F_{OVP}(z), \quad (3)$$

where $P_{OVP}^{MPL}(z)$ represents the overlap-corrected P-MPL RCS profiles.

In this work, the experimental procedure to obtain F_{OVP} is based on the comparison of the $P^{MPL}(z)$ to either
 the Polly RCS profiles, $P^{Polly}(z)$, or the MARTHA ones, $P^{MARTHA}(z)$, which are both used as reference

215 under relatively clean and mostly clear conditions. The Polly and MARTHA lidars present the advantage
 in contrast to P-MPL system that the OVP function can be experimentally determined using their Raman
 channels (Wandinger and Ansmann, 2002). The P-MPL overlap function is thus calculated in terms of the
 ratio between the P-MPL and Polly/MARTHA RCS profiles, i.e.,

$$F_{OVP}(z) = P^{MPL}(z)/P^{ref}(z), \quad (4)$$

220 where $P^{ref}(z)$ denotes the reference RCS profiles as obtained from either Polly, $P^{Polly}(z)$, or MARTHA,
 $P^{MARTHA}(z)$, measurements. Both sets of RCS profiles are normalized at a given height (higher than the
 OVP altitude range under aerosol-free conditions), z_{norm} , and then $F_{OVP}(z)$ can be derived using **Eq. 3**. In
 particular, the full-OVP is conservatively obtained at the normalization height $z_{norm} = 9.5$ km a.g.l., being
 $F_{OVP}(z) = 1$ at $z \geq z_{norm}$. Errors associated to the estimation of $F_{OVP}(z)$ using this experimental approach
 225 are described in **Annex A**. Night-time lidar observations performed under relatively clean conditions at the
 Leipzig station (AERONET AOD < 0.1 and AE > 1.2) were used for the P-MPL OVP determination. In
 particular, two time periods were selected in coincidence with either Polly or MARTHA observations in
 order to provide an extended comparison analysis using diverse reference lidar systems under different lidar
 operational conditions.

230 **2.4 Retrieval of the aerosol optical properties: Particle backscatter coefficient, and both volume and particle linear depolarization ratios**

Once the OVP-corrected RCS is obtained from **Eq. 3**, the particle backscatter coefficient (PBC), β_p (km^{-1}
 sr^{-1}) can be derived applying the Klett-Fernald (KF) algorithm (Fernald, 1984; Klett, 1985) by constraining
 the lidar ratio (LR, extinction-to-backscatter ratio) with the AERONET Aerosol Optical Depth (AOD)
 235 (elastic KF solution) (Marenco et al., 1997); hence, an effective LR, S_a^{eff} , is also obtained after
 convergence.

The particle linear depolarization ratio (PLDR), δ_p , can be determined as follows,

$$\delta_p = \frac{R \delta^V (1 + \delta_{mol}) - \delta_{mol} (1 + \delta^V)}{R (1 + \delta_{mol}) - (1 + \delta^V)} \quad (5)$$

where R is the backscattering ratio ($R = \frac{(\beta_m + \beta_p)}{\beta_m}$, being β_m the molecular backscattering coefficient), δ^V
 240 is the volume linear depolarization ratio (VLDR), and δ_{mol} is the molecular depolarization ratio. For P-
 MPL systems, $\delta_{mol} = 0.0037$ that is almost independent on atmospheric temperature (relative uncertainty
 < 0.1%), as their FWHM is less than 0.2 nm (Behrendt and Nakamura, 2002). The PLDR is a lidar parameter
 widely used for defining the aerosol type (Burton et al., 2012; Gross et al., 2013), and for discriminating
 the particle size mode in some aerosol mixtures (Mamouri and Ansmann, 2017; Córdoba-Jabonero et al.,
 245 2018), among others. The determination of PBC is mainly depending on the OVP correction, as will be
 discussed in **Sect. 3.3**, and hence, the PLDR is also affected by OVP as well. Therefore, a good knowledge
 of the OVP function for the specific P-MPL system is also needed to obtain high-quality PBC and PLDR
 profiles.

The volume linear depolarization ratio (VLDR), δ^V , can be determined in relation with the P-MPL depolarization ratio, δ^{MPL} (Mishchenko and Hovenier, 1995; Gimmestad, 2008). Looking at the formulae shown in Flynn et al. (2007; see their Eq. 1.8), δ^V can be easily expressed as

$$\delta^V = \frac{\delta^{MPL}}{\delta^{MPL}+1} = \frac{P_{cross}}{P_{co}+P_{cross}}, \quad (6)$$

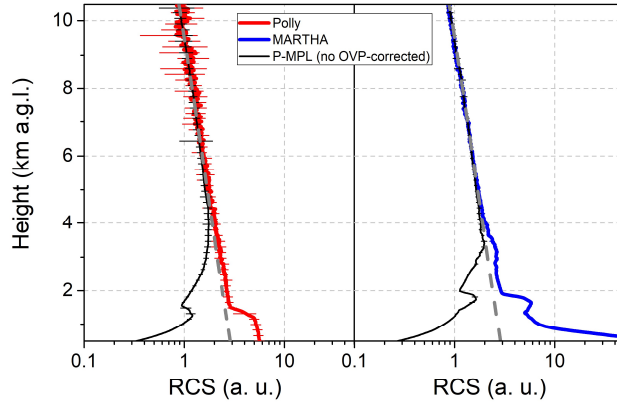
i.e., the **Eq. 2** is obtained, where δ^{MPL} is defined as the ratio between P_{cross} and P_{co} (the two polarized RCS as described in **Sect. 2.2.1**). Since the OVP function is equally applied to both those signals, the VLDR is unaffected by the OVP correction; however, it actually affects, together with the PBC, the PLDR estimation (see **Eq. 5**). Therefore, the VLDR for the P-MPL system was also experimentally evaluated in comparison with that derived from Polly lidar measurements, for instance, similarly to the approach shown by Córdoba-Jabonero et al. (2013). This experimental polarization correction is based on real measurements as an alternative (see **Sect. 3.2**), due to the unavailability of applying the special and specific methods for polarization calibration within MPLNET, as those described in Welton et al. (2018).

All those variables are height-resolved, but the altitude dependence is omitted for simplicity. A dust case occurring for the night on 29-30 June 2019 at the Leipzig station is selected for that purpose (in particular, the dust intrusion as observed over Leipzig in June 2019 is widely characterized in Córdoba-Jabonero et al., 2021).

265 3 Results

3.1 Experimental overlap function F_{OVP}

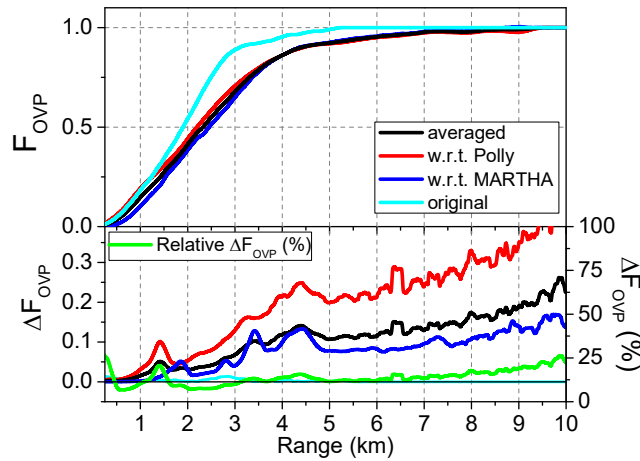
P-MPL observations were carried out from 6 June to 26 July 2019 at the Leipzig station during the field campaign. Simultaneous P-MPL and Polly/MARTHA measurements as performed under relatively clean conditions were selected for estimating the OVP function. The first comparison analysis corresponded to 270 12 hourly-averaged P-MPL and Polly RCS profiles within the night-time period from 28 June 2019 at 18UT to 29 June 2019 at 05UT (day-time values on 28 June at 18UT: AOD=0.10, Ångstrom exponent AE=1.59). The second one was related to the MARTHA night-time RCS measurements as averaged for 4 hours from 23 July 2019 at 21UT to 24 July 2019 at 00UT (day-time values on 23 July at 18UT: AOD=0.09, AE=1.33); P-MPL RCS profiles were also averaged during that same period for comparison. **Figure 1** shows the uncorrected by overlap P-MPL RCS profiles in comparison with the reference Polly (left panel) and MARTHA (right panel) ones for both those particular periods. The part of the P-MPL RCS profiling to be OVP-corrected is clearly highlighted ranging from the surface up to around 6 km height. Next, the experimental estimation of F_{OVP} for the P-MPL system is analysed in terms of the OVP-corrected RCS as obtained by applying each of those experimentally-estimated F_{OVP}^{Polly} and F_{OVP}^{MARTHA} (see **Sect. 2.3.1**), 275 including also a comparison with the original one, $F_{OVP}^{original}$ (as provided by the manufacturer). 280



285 **Figure 1:** Comparison of the normalized (left) reference Polly (red line; for clarity, the 12 P-MPL and Polly RCS profiles, from 28 June 18UT to 29 June 05UT, were averaged) and (right) MARTHA (blue line; 4 P-MPL and MARTHA RCS profiles, from 23 July 21UT to 24 July 00UT, were averaged) w.r.t. the uncorrected by overlap P-MPL profiles (black lines). Normalization height at 9.5 km a.g.l. The aerosol-free background signal is shown by a grey dashed line.

Figure 2 shows the experimental OVP functions, $F_{OVP}(z)$, as obtained from the comparison of the P-MPL RCS profiles w.r.t. Polly and MARTHA lidar measurements (top panel, F_{OVP}^{Polly} in red, and F_{OVP}^{MARTHA} in blue) (see **Eq. 4**) together with $F_{OVP}^{original}$; associated errors are also shown in the bottom panel. In addition, as both those OVP functions were obtained in two different days, temperature-related changes could be produced in the OVP estimation. Hence, the averaged $F_{OVP}^{av}(z)$ between both OVP functions is also calculated, and shown together the absolute and relative errors in **Fig. 2**, top and bottom panels, respectively). Details on the OVP error processing are described in **Annex A**. By comparing with the original OVP function, large discrepancies can be clearly observed, highlighting the change of $F_{OVP}(z)$ with time, mostly in the relevant 1-5 km height-range. Regarding the OVP functions F_{OVP}^{Polly} and F_{OVP}^{Martha} , differences are also found, mostly in the near-field range up to around 3 km height. However, by using $F_{OVP}^{av}(z)$ instead of one of two others for P-MPL RCS correction, its relative error is just $14 \pm 5\%$ in average from 0.3 up to 10 km height (see **Fig. 2-bottom**). Taking into account these errors, $F_{OVP}^{av}(z)$ can be the OVP function used for correcting the P-MPL RCS profiles at near-field heights, following the expression in **Eq. 3**, as it seems to be the best proxy for OVP correction of the P-MPL RCS profiles.

290
 300



305 **Figure 2: (Top)** Experimental overlap functions, F_{OVP} , as obtained for two different days from the ratio between the P-MPL RCS profiles w.r.t. the Polly (F_{OVP}^{Polly} , red) and MARTHA (F_{OVP}^{MARTHA} , blue) ones, together with the averaged function (F_{OVP}^{av}) of both of them (black line); the original overlap function as provided by the manufacturer, $F_{OVP}^{original}$, is also included (cyan line). (Bottom) Errors, ΔF_{OVP} , associated to the OVP-function estimation for each comparison case: P-MPL w.r.t. Polly (red), P-MPL w.r.t. MARTHA (blue), and the averaged OVP function of both of them (black); the error for $F_{OVP}^{original}$ (cyan) and the relative error for F_{OVP}^{av} (green line) are also included.

310

The previous uncorrected and OVP-corrected P-MPL RCS profiles by using both F_{OVP}^{av} and $F_{OVP}^{original}$ are shown in **Figure 3**. Slightly differences are observed for the P-MPL RCS profiles as compared to those Polly and MARTHA ones by using F_{OVP}^{av} , despite it was calculated from averaging F_{OVP}^{Polly} and F_{OVP}^{MARTHA} , which were obtained from measurements on different days (only almost one month between them). Large differences are clearly found when $F_{OVP}^{original}$ is applied, mostly between 1.5 and 3 km height, evidencing that the OVP function as provided by the manufacturer is not applicable after some time for aerosol research, being necessary an regular OVP determination, as performed and described in this work. Once the P-MPL RCS profiles are OVP-corrected, the optical properties of the aerosols can be retrieved using inversion algorithms. OVP-induced effects in the inversion of the aerosol optical properties are analysed in

315

Sect. 3.3.

320

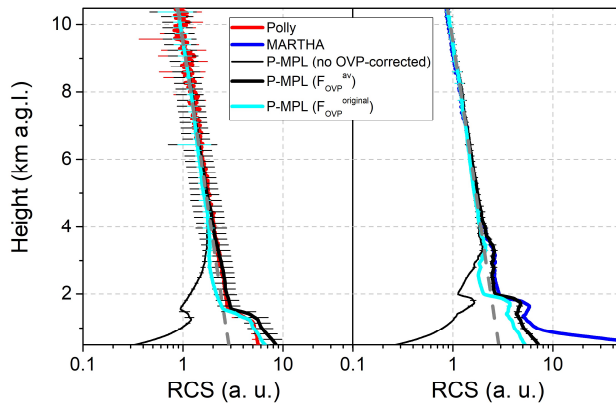


Figure 3: OVP-corrected (black thick lines) P-MPL RCS profiles by using F_{OVP}^{av} function and the uncorrected RCS ones (black thin lines), w.r.t. (Left) Polly (red line) and (Right) MARTHA (blue line) RCS profiles, together with the OVP-corrected ones by $F_{OVP}^{original}$ (cyan lines).

325

3.2 Volume linear depolarization ratio (VLDR)

Before analysing the OVP impact in the retrieval of the aerosol optical properties, the VLDR is also examined. As stated before, despite the VLDR is unaffected by the OVP correction, it actually affects, together with the PBC, β_p , the PLDR, δ_p , estimation (see Sect. 2.4).

330 The P-MPL VLDR is calculated using Eq. 6 and compared with that derived from Polly measurements as reference, since TROPOS follows all quality assurance efforts regarding polarization lidar calibration tests in the Polly systems as recommended by EARLINET (Freudenthaler et al., 2008, 2016). A dust outbreak case observed at Leipzig site for the night on 29-30 June 2019 is examined for that purpose. Figure 4 shows the VLDR as obtained from both the δ_{MPL}^V and δ_{Polly}^V profiles as averaged from 18 to 23 UT on 29 June and
 335 from 00 to 05 UT on 30 June (for clarity, only averaged δ^V profiles are shown). The dust signature is clearly marked, showing a dust layer clearly confined between 3 and 6 km height, with a higher variability for the second interval due to the decay of dusty conditions at the end of that period, as reflected by a larger error uncertainty in time averaging. In overall, despite δ_{MPL}^V values seems to be higher than those δ_{Polly}^V , peaking between 0.11 and 0.14 in the dust layer, they are within the error range. Hence, the VLDR was averaged
 340 within several aerosol-free height-intervals, below and above that defined dust layer, to analyse potential changes and offsets. Those mean δ^V values (and their standard deviation, SD) are shown in Table 2.

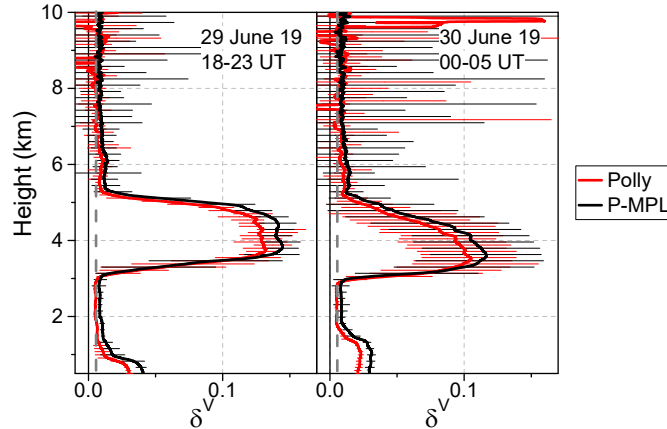


Figure 4: Volume linear depolarization ratio (VLDR), δ^V , as obtained from both the P-MPL (black line) and Polly (15-p smoothed red line) measurements carried out on: (left) 29 June 2019, as averaged from 18 to 23 UT,
 345 and (right) 30 June 2019, as averaged from 00 to 05 UT (error bars are also shown in black and red, respectively). The aerosol-free background δ^V is marked by a grey dashed line.

Table 2: Mean VLDR values together their standard deviation (SD) (and their relative SD error, in %) as obtained from the P-MPL and Polly measurements (δ_V^{MPL} and δ_V^{Polly} profiles) for aerosol-free height-intervals
 350 on 29-30 June 2019.

Height intervals (km)	δ^V , mean \pm SD (%SD)	
	P-MPL	Polly
1.5-2.5	0.0096 \pm 0.0016 (16.6)	0.0057 \pm 0.0002 (3.4)
7.0-8.0	0.0088 \pm 0.0010 (10.8)	0.0057 \pm 0.0037 (65.9)
8.0-9.0	0.0083 \pm 0.0016 (19.7)	0.003 \pm 0.016 (> 100)
Height-averaged	0.0089 \pm 0.0005 (6.0)	0.0049 \pm 0.0011 (23.1)

Looking at the results, δ_{Polly}^V presents larger errors than those for δ_{MPL}^V , as associated to a lower signal-to-noise ratio as height increases for the Polly measurements (no smoothing applied). This is reflected by the higher relative error (%SD) found for the Polly VLDR (23%) w.r.t. to that for the P-MPL (6%) when all the aerosol-free height-intervals are considered, being the mean δ^V values of 0.0089 ± 0.0005 (%SD: 6%) and 0.0049 ± 0.0011 (%SD: 23%), respectively, for the P-MPL and Polly VLDR. As a result, a constant offset, Δ ($= \delta_{Polly}^V - \delta_{MPL}^V$), can be assumed between δ_{MPL}^V and δ_{Polly}^V , obtaining $\Delta = -0.0040 \pm 0.0016$. This offset can represent a correction to account for any slight mismatch in the transmitter and detector polarization planes and any impurity of the laser polarization state (Sassen, 2005), as also found in Córdoba-Jabonero et al. (2013) by characterizing the VLDR of a relatively older version (MPL-4) of the polarized MPL systems. Therefore, the P-MPL VLDR must be also corrected by that offset using the expression:

$$\delta_{MPL}^{V\ corr} = \delta_{MPL}^V + \Delta, \quad (7)$$

where $\delta_{MPL}^{V\ corr}$ is the corrected P-MPL VLDR profile, and δ_{MPL}^V is that VLDR as obtained from **Eq. 2**. Regarding the dust layer extended between 3.5 and 5.0 km height, as expected, a similar δ^V value to that obtained for the Polly VLDR ($\delta_{Polly}^V = 0.11 \pm 0.02$) is estimated for the corrected P-MPL VLDR, i.e., $\delta_{MPL}^{V\ corr} = 0.12 \pm 0.02$, as averaged within that dust layer. The corresponding PLDR to those δ^V are around 0.3 (as shown in **Sect. 3.3**), which are typical PLDR values for dust (Burton et al., 2012; Gross et al., 2013).

3.3 Particle backscatter coefficient (PBC) and particle linear depolarization ratio (PLDR)

The effect of the OVP correction on the P-MPL RCS is also analysed regarding the retrieval of the KF-derived β_p profiles, as obtained by applying both $F_{OVP}^{original}$ and F_{OVP}^{av} to the RCS. A dust event as observed at Leipzig on the night from 29 to 30 June 2019 (the same dust case as previously exposed in **Sect. 3.2**) is selected for that purpose. In addition, both PLDR, δ_p (see **Eq. 5**), and VLDR, δ^V (see **Eqs. 6 and 7**, Δ offset corrected) are estimated. The OVP-induced effect is illustrated, in particular, using the vertical hourly-averaged profiling observed on 29 June 2019 at 20-21 UT, corresponding to a well-separated two-layer dust case (dust optical depth of 0.061). **Figures 5 and 6** show the vertical profiles of β_p and δ_p (and δ^V), respectively, depending on the F_{OVP} applied, as retrieved from the P-MPL measurements together to those derived from Polly ones for the selected case.

Both P-MPL and Polly datasets show a dust layer clearly confined between around 3.5 and 5.0 km height. For comparison, in addition to the AOD-constrained KF solution for the PBC (reference height at 6.0 km, and reference backscatter coefficient of $10^{-7} \text{ Mm}^{-1} \text{ sr}^{-1}$) using $S_a^{eff} = 43 \text{ sr}$ (that obtained from Polly elastic

measurements) (see **Figs. 5a**), β_p is also retrieved by using the Raman-derived LR ($S_a^{Raman} = 60$ sr) for that dust layer as obtained from the night-time Polly Raman measurements (data not shown) (see **Figs. 5b**).

385 **Table 3: Dust layer-averaged PBC, $\overline{\beta}_p$ ($\text{Mm}^{-1} \text{sr}^{-1}$), and PLDR, $\overline{\delta}_p$, and the integrated backscatter, B (10^{-3}sr^{-1}), values, as obtained from P-MPL β_p and δ_p profiles on 29 June 2019 at 20-21 UT in dependence of the F_{OVP} applied for both the KF solutions (using S_a^{eff} and S_a^{Raman}). Corresponding Polly values are also included.**

F_{OVP}	P-MPL						Polly		
	$S_a^{eff} = 43$ sr			$S_a^{Raman} = 60$ sr			$S_a^{eff} = 43$ sr		
	$\overline{\beta}_p$	B	$\overline{\delta}_p$	$\overline{\beta}_p$	B	$\overline{\delta}_p$	$\overline{\beta}_p$	B	$\overline{\delta}_p$
F_{OVP}^{av}	0.93 ± 0.17	1.41 ± 0.16	0.32 ± 0.01	0.89 ± 0.15	1.35 ± 0.16	0.33 ± 0.01			
F_{OVP}^{Polly}	0.92 ± 0.16	1.40 ± 0.27	0.32 ± 0.01	0.88 ± 0.14	1.33 ± 0.27	0.33 ± 0.01	0.72 ± 0.16	1.08	0.33 ± 0.01
F_{OVP}^{MARTHA}	0.94 ± 0.17	1.43 ± 0.10	0.32 ± 0.01	0.90 ± 0.15	1.36 ± 0.10	0.32 ± 0.01	0.16		0.01
$F_{OVP}^{original}$	0.87 ± 0.14	1.32 ± 0.05	0.33 ± 0.01	0.83 ± 0.12	1.26 ± 0.08	0.34 ± 0.02			

Regarding the dust layer, relatively small differences are found between Polly and P-MPL β_p profiles (see **Fig. 5**), at least within error uncertainties. In order to assess those differences between both datasets, the layer-averaged PBC, $\overline{\beta}_p$ ($\text{Mm}^{-1} \text{sr}^{-1}$), and the integrated backscatter, B (sr^{-1}), for this 3.5-5.0-km dust layer were calculated to be used as a proxy of the degree of agreement. Derived $\overline{\beta}_p$ and B values in dependence of F_{OVP} for both the KF solutions (using either S_a^{eff} or S_a^{Raman}) are shown in **Table 3**. In general, $\overline{\beta}_p$ and B are higher for P-MPL w.r.t. Polly retrievals. Concerning the KF solutions for P-MPL profiles, a better agreement is achieved when the S_a^{Raman} of 60 sr is applied (no AOD-constrain), i.e., lower differences for $\overline{\beta}_p$ and B are found w.r.t. Polly-retrieved values.

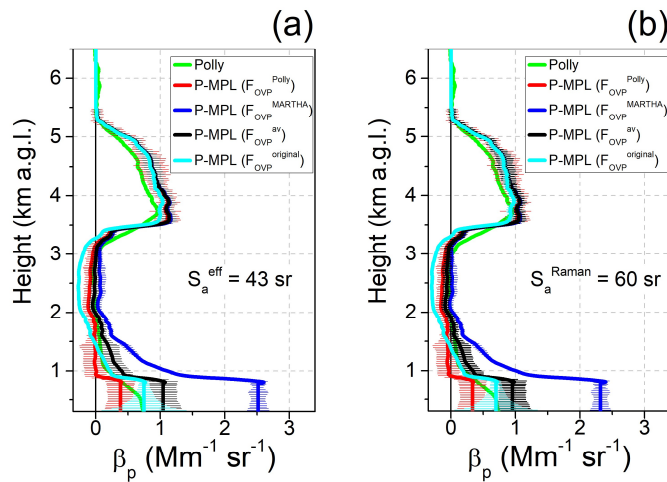
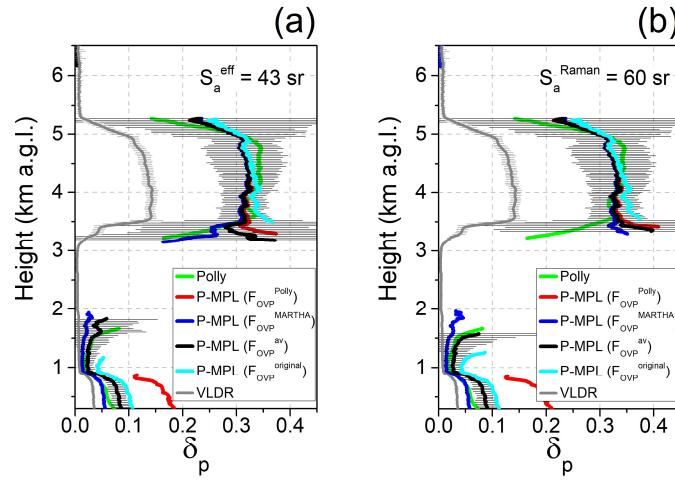


Figure 5: Dust case as observed on 29 June 2019 at 20:00-21:00 UT over Leipzig: Vertical particle backscatter coefficient (PBC), β_p , as retrieved in dependence of the OVP function applied to the P-MPL RCS: F_{OVP} w.r.t.

400 to Polly (red) and MARTHA (blue) data and both the F_{OVP}^{av} (black) and $F_{OVP}^{original}$ (cyan) by using the KF solution with (a) the elastic AOD-constrained LR ($S_a^{eff} = 43$ sr), and (b) the Raman-retrieved LR ($S_a^{Raman} = 60$ sr) for the dust layer. Corresponding Polly-retrieved β_p profiles are also included (green lines).

Nevertheless, the KF retrieval is mostly affected at near-field ranges (up to 3 km height) (see Fig. 5), as expected, since the OVP correction is rather relevant at those ranges. Negative β_p values are predominantly
 405 found for the scenarios when the RCS is OVP-corrected by F_{OVP}^{Polly} and $F_{OVP}^{original}$, being more pronounced when the S_a^{Raman} is applied, since the LR to be applied in this height-interval must be closer to the elastic S_a^{eff} of 43 sr. The best fitting seems to be achieved by using F_{OVP}^{MARTHA} and F_{OVP}^{av} . Among those, however, results show that β_p profiles are in a better agreement by using F_{OVP}^{av} as compared to those Polly-derived β_p at ranges from around 1 km down (see Fig. 5). Relative $\beta_p[F_{OVP}^{av}]$ errors of 10-20% are obtained.



410 **Figure 6:** The same as Fig. 5, but for the vertical particle linear depolarization ratio (PLDR), δ_p , as retrieved from each $\beta_p[F_{OVP}]$ as shown in Fig. 5, and the VLDR, δ^V (grey line). The corresponding Polly-retrieved δ_p profile is also included (green line). For clarity, only error bars are marked for $\delta_p[F_{OVP}^{av}]$ (black) and δ_p^{Polly} (green).

415 By examining the PLDR profiles, the dust signature is also clearly marked between around 3.5 and 5.0 km height, i.e., typical δ_p values for dust of around 0.3 are found (see Table 3), indicating a predominance of coarse particles. No differences are found between Polly and P-MPL PLDR profiles for that layer (see Fig. 6), with mean δ_p values of 0.33 ± 0.01 (Polly) and 0.32 - 0.34 ± 0.02 (P-MPL, depending on the F_{OVP} applied and the LR used) (see Table 3).

4 Conclusions

A comprehensive two-month field intercomparison campaign has been performed in summer 2019 to characterize the performance of a polarized Micro-Pulse Lidar (P-MPL) system, and to check the quality of the retrieved aerosol products. Atmospheric observations of the P-MPL system have been examined

425 against those from two reference EARLINET lidars (Polly and MARTHA), which are operative at Leipzig
site (Germany, 51.4°N 12.4°E, 125 m a.s.l.) as managed by TROPOS. In particular, an experimental
assessment in terms of the overlap (OVP) correction and its impact in the retrieval of the aerosol optical
properties has been achieved. Furthermore, the volume linear depolarization ratio (VLDR) has also been
cross-checked and corrections applied, allowing an accurate retrieval. The aim of this work has been
430 focused on the determination of the lidar-specific true OVP function and on investigating the accuracy of
both the retrieved particle backscatter coefficient (PBC) and particle linear depolarization ratio (PLDR)
profiles.

It has been highlighted that the OVP function as delivered by the P-MPL manufacturer cannot be long used.
The reasons are manifold, but an suitable estimation of the OVP function should be recommended for the
435 MPL system. The experimental procedure to determine the OVP function for the P-MPL system has been
described in the basis of the comparison to reference lidars. The optimal OVP function for correcting the
P-MPL measurements has been obtained, together with its uncertainties, under clean observational
conditions from simultaneous P-MPL and Polly/MARTHA observations, and compared with the original
one as provided by the manufacturer. In addition, depending on the OVP function applied, the OVP
440 correction-induced effects in the retrieval of both the PBC and PLDR for the P-MPL system have been
analysed for two KF solutions by using either the elastic (AOD-constrained) or the Raman-provided lidar
ratios in comparison with those PBC and PLDR retrievals as obtained from simultaneous Polly
observations. A dust case as observed at Leipzig is analyzed for that purpose. Additionally, despite the
VLDR is OVP-unaffected, it has been also examined in comparison with the Polly VLDR regarding its
445 effect in the PLDR determination. A suitable VLDR profile has been obtained, being only needed to be
corrected by a small offset value, which has been also estimated. Once P-MPL measurements were
optimally OVP-corrected and the VLDR adjusted, both the PBC and PLDR profiles have been accurately
derived by using the KF solution.

In overall, as a systematic requirement for lidar systems, an adequate OVP function determination and
450 VLDR testing analysis is needed to be performed in a regular basis in order to correct the P-MPL
measurements and, hence, to derive suitable aerosol products (backscatter, depolarization, extinction). The
procedure described in this study can be useful to be applied to similar P-MPL systems that cannot regularly
apply the established MPLNET calibrations. Moreover, such kind of efforts should be addressed on the
way to combine all existing networks in Europe (EARLINET), Asia (AD-NET), Latina America
455 (LALINET), and also MPLNET within the future vision of GAW (Global Atmospheric Watch) Aerosol
Lidar Observations Network (GALION).

Annex A

The experimental overlap (OVP) function, $F_{OVP}^{ref}(z)$, is obtained from the expression

$$F_{OVP}^{ref}(z) = P^{MPL}(z)/P^{ref}(z), \quad (A.1)$$

460 where $P^{MPL}(z)$ are the P-MPL RCS profiles, which are compared against those reference lidar measurements, $P^{ref}(z)$ (*ref* denotes either Polly or MARTHA) using the experimental approach as described in this work.

The error associated to the determination of the OVP function, ΔF_{OVP} , is obtained from error propagation calculations of the **Eq. A.1**. In this sense, it can be expressed as (*z*-dependence is omitted for simplicity, hereafter)

$$\Delta F_{OVP}^{ref} = F_{OVP}^{ref} \times \left[\frac{\Delta P^{MPL}}{P^{MPL}} + \frac{\Delta P^{ref}}{P^{ref}} \right], \quad (\text{A.2})$$

where ΔP^{MPL} and ΔP^{ref} are, respectively, the errors related to P^{MPL} and P^{ref} .

ΔP^{MPL} can be estimated as composed of two error contributions: one associated to instrumental corrections (energy fluctuations, instrumental calibrations, solar background, ...), ε^{MPL} , as described in Welton and Campbell (2002), and another one reflecting the atmospheric variability within the time-averaging performed of the P^{MPL} profiles, which is expressed by the standard deviation, sd^{MPL} ; hence, it can be obtained from the expression

$$\Delta P^{MPL} = \sqrt{(\varepsilon^{MPL})^2 + (sd^{MPL})^2}. \quad (\text{A.3})$$

Errors associated to the reference lidar measurements, ΔP^{ref} (*ref* is for either Polly or MARTHA), are represented by the standard deviation, as obtained from the corresponding time-averaging of P^{ref} profiles.

In this work, the averaged function between F_{OVP}^{Polly} and F_{OVP}^{MARTHA} is also calculated, i.e.,

$$F_{OVP}^{av} = \frac{F_{OVP}^{Polly} + F_{OVP}^{MARTHA}}{2}, \quad (\text{A.4})$$

being the error related to this function, ΔF_{OVP}^{av} , estimated as

$$\Delta F_{OVP}^{av} = \sqrt{\left(\frac{\Delta F_{OVP}^{Polly}}{2} \right)^2 + \left(\frac{\Delta F_{OVP}^{MARTHA}}{2} \right)^2}, \quad (\text{A.5})$$

480 where ΔF_{OVP}^{ref} (*ref* denotes either Polly or MARTHA) is the error as obtained from **Eq. A.2**.

Data availability. All data generated and analysed for this study are available from the authors upon reasonable request.

Author Contributions. CC-J and AA designed the study and wrote the original draft paper. CC-J, AA, CJ and HB provided data. CC-J and CJ performed data analysis with contributions from AA, HB, M-AL-C and RE. All authors reviewed and edited the final version of the manuscript. All the authors agreed to the final version of the paper.

Competing interests. The authors declare that they have no conflict of interest.

Acknowledgements

This work was supported by the Spanish Ministry of Science, Innovation and Universities (MCIU) under grants PRX18/00137 (Programa "Salvador de Madariaga") and CGL2017-90884-REDT (ACTRIS-Spain), the Spanish Ministry of Science and Innovation (MICINN) (grant PID2019-104205GB-C21), and the H2020 program from the European Union (ACTRIS, GA n. 871115). M-AL-C is supported by the INTA predoctoral contract programme. We thank MPLNET for its support even though this study was not part of MPLNET activities. The MPLNET project is funded by the NASA Radiation Sciences Program and Earth Observing System.

References

- Althausen, D., Engelmann, R., Baars, H., Heese, B., Ansmann, A., Müller, D. and Komppula, M.: Portable Raman Lidar PollyXT for Automated Profiling of Aerosol Backscatter, Extinction, and Depolarization, *J. Atmos. Oceanic Technol.*, 26 (11), 2366-2378, <https://doi.org/10.1175/2009JTECHA1304.1>, 2009.
- Amiridis, V., E. Marinou, A. Tsekeri, U. Wandinger, A. Schwarz, E. Giannakaki, R. Mamouri, P. Kokkalis, I. Biniotoglou, S. Solomos, T. Herekakis, S. Kazadzis, E. Gerasopoulos, D. Balis, A. Papayannis, C. Kontoes, K. Kourtidis, N. Papagiannopoulos, L. Mona, G. Pappalardo, O. Le Rille, and A. Ansmann: LIVAS: a 3-D multi-wavelength aerosol/cloud climatology based on CALIPSO and EARLINET, *Atmos. Chem. Phys.*, 15, 7127-7153, <https://doi.org/10.5194/acp-15-7127-2015>, 2015.
- Ansmann, A., Tesche, M., Seifert, P., Groß, S., Freudenthaler, V., Apituley, A., Wilson, K. M., Serikov, I., Linné, H., Heinold, B., Hiebsch, A., Schnell, F., Schmidt, J., Mattis, I., Wandinger, U. and Wiegner, M.: Ash and fine-mode particle mass profiles from EARLINET-AERONET observations over central Europe after the eruptions of the Eyjafjallajökull volcano in 2010, *J. Geophys. Res.-Atmos.*, 116 (D20), <https://doi.org/10.1029/2010JD015567>, 2011.
- Baars, H., Kanitz, T., Engelmann, R., Althausen, D., Heese, B., Komppula, M., Preißler, J., Tesche, M., Ansmann, A., Wandinger, U., Lim, J.-H., Ahn, J. Y., Stachlewska, I. S., Amiridis, V., Marinou, E., Seifert, P., Hofer, J., Skupin, A., Schneider, F., Bohlmann, S., Foth, A., Bley, S., Pfüller, A., Giannakaki, E., Lihavainen, H., Viisanen, Y., Hooda, R. K., Pereira, S. N., Bortoli, D., Wagner, F., Mattis, I., Janicka, L., Markowicz, K. M., Achtert, P., Artaxo, P., Pauliquevis, T., Souza, R. A. F., Sharma, V. P., van Zyl, P. G., Beukes, J. P., Sun, J., Rohwer, E. G., Deng, R., Mamouri, R.-E. and Zamorano, F.: An overview of the first decade of PollyNET: an emerging network of automated Raman-polarization lidars for continuous aerosol profiling, *Atmos. Chem. Phys.*, 16 (8), 5111–5137, <https://doi.org/10.5194/acp-16-5111-2016>, 2016.
- Baars, H., Ansmann, A., Ohneiser, K., Haarig, M., Engelmann, R., Althausen, D., Hanssen, I., Gausa, M., Pietruczuk, A., Szkop, A., Stachlewska, I. S., Wang, D., Reichardt, J., Skupin, A., Mattis, I., Trickl, T., Vogelmann, H., Navas-Guzmán, F., Haeefe, A., Acheson, K., Ruth, A. A., Tatarov, B., Müller, D., Hu, Q., Podvin, T., Goloub, P., Veselovskii, I., Pietras, C., Haeffelin, M., Fréville, P., Sicard, M., Comerón, A., Fernández García, A. J., Molero Menéndez, F., Córdoba-Jabonero, C., Guerrero-Rascado, J. L., Alados-Arboledas, L., Bortoli, D., Costa, M. J., Dionisi, D., Liberti, G. L., Wang, X., Sannino, A., Papagiannopoulos, N., Boselli, A., Mona, L., D'Amico, G., Romano, S., Perrone, M. R., Belegante, L., Nicolae, D., Grigorov, I., Gialitaki, A., Amiridis, V., Soupiona, O., Papayannis, A., Mamouri, R.-E., Nisantzi, A., Heese, B., Hofer, J., Schechner, Y. Y., Wandinger, U., and Pappalardo, G.: The unprecedented

- 2017–2018 stratospheric smoke event: decay phase and aerosol properties observed with the EARLINET, *Atmos. Chem. Phys.*, 19, 15183-15198, doi.org/10.5194/acp-19-15183-2019, 2019.
- 530 Barbosa, H. M. J., Lopes, F. J. S., Silva, A., Nisperuza, D., Barja, B., Ristori, P., Gouveia, D. A., Jimenez, C., Montilla, E., Mariano, G. L., Landulfo, E., Bastidas, A. and Quel, E. J.: The first ALINE measurements and intercomparison exercise on lidar inversion algorithms, *Opt. Pura Apl.*, 47 (2), 99-108, <https://doi.org/10.7149/OPA.47.2.99>, 2014.
- 535 Behrendt, A. and Nakamura, T.: Calculation of the calibration constant of polarization lidar and its dependency on atmospheric temperature, *Opt. Express*, 10 (16), 805–817, <https://doi.org/10.1364/OE.10.000805>, 2002.
- Belegante, L., Bravo-Aranda, J. A., Freudenthaler, V., Nicolae, D., Nemuc, A., Ene, D., Alados-Arboledas, L., Amodeo, A., Pappalardo, G., D’Amico, G., Amato, F., Engelmann, R., Baars, H., Wandinger, U., Papayannis, A., Kokkalis, P. and Pereira, S. N.: Experimental techniques for the calibration of lidar depolarization channels in EARLINET, *Atmos. Meas. Tech.*, 11 (2), 1119-1141, <https://doi.org/10.5194/amt-11-1119-2018>, 2018.
- 540 Berkoff, T. A., Welton, E. J., Campbell, J.R., Scott, V.S., and Spinhirne, J. D.: Investigation of Overlap Correction Techniques for the Micro-Pulse Lidar NETWORK (MPLNET), 2003 IEEE International Geoscience and Remote Sensing Symposium (2003 IGARSS). Proceedings (IEEE Cat. No. 03CH37477), 4395-4397, <https://doi.org/10.1109/IGARSS.2003.1295527>, 2003.
- 545 Böckmann, C., Wandinger, U., Ansmann, A., Bösenberg, J., Amiridis, V., Boselli, A., Delaval, A., Tomasi, F. D., Frioud, M., Grigorov, I. V., Hågård, A., Horvat, M., Iarlori, M., Komguem, L., Kreipl, S., Larchevêque, G., Matthias, V., Papayannis, A., Pappalardo, G., Rocadenbosch, F., Rodrigues, J. A., Schneider, J., Shcherbakov, V. and Wiegner, M.: Aerosol lidar intercomparison in the framework of the EARLINET project. 2. Aerosol backscatter algorithms, *Appl. Opt.*, 43 (4), 977-989, <https://doi.org/10.1364/AO.43.000977>, 2004.
- 550 Bohlmann, S., Shang, X., Giannakaki, E., Filioglou, M., Saarto, A., Romakkaniemi, S. and Komppula, M.: Detection and characterization of birch pollen in the atmosphere using multi-wavelength Raman lidar in Finland, *Atmos. Chem. Phys.*, 19 (23), 14559, <https://doi.org/10.5194/acp-2019-635>, 2019.
- 555 Bravo-Aranda, J. A., Baumgardner, D., Guerrero-Rascado, J. L., Veselovskii, I., Lyamani, H., Valenzuela, A., Olmo, F. J., Titos, G., Andrey, J., Chaikovskiy, A., Dubovik, O., Gil-Ojeda, M. and Alados-Arboledas, L.: A comparative study of aerosol microphysical properties retrieved from ground-based remote sensing and aircraft in situ measurements during a Saharan dust event, *Atmos. Meas. Tech.*, 9 (3), 1113-1113, 2016.
- 560 Burton, S. P., Ferrare, R. A., Hostetler, C. A., Hair, J. W., Rogers, R. R., Obland, M. D., Butler, C. F., Cook, A. L., Harper, D. B. and Froyd, K. D.: Aerosol classification using airborne High Spectral Resolution Lidar measurements - methodology and examples, *Atmos. Meas. Tech.*, 5 (1), 73-98, <https://doi.org/10.5194/amt-5-73-2012>, 2012.
- Burton, S. P., Vaughan, M. A., Ferrare, R. A. and Hostetler, C. A.: Separating mixtures of aerosol types in airborne High Spectral Resolution Lidar data, *Atmos. Meas. Tech.*, 7 (2), 419-436, <https://doi.org/10.5194/amt-7-419-2014>, 2014.
- 565 Campbell, J. R., Hlavka, D. L., Welton, E. J., Flynn, C. J., Turner, D. D., Spinhirne, J. D., Scott, V. S. and Hwang, I. H.: Full-Time, Eye-Safe Cloud and Aerosol Lidar Observation at Atmospheric Radiation

- Measurement Program Sites: Instruments and Data Processing, *J. Atmos. Oceanic Technol.*, 19 (4), 431-442, [https://doi.org/10.1175/1520-0426\(2002\)019<0431:FTESCA>2.0.CO;2](https://doi.org/10.1175/1520-0426(2002)019<0431:FTESCA>2.0.CO;2), 2002.
- 570 Campbell, J. R. and Sassen, K.: Polar stratospheric clouds at the South Pole from 5 years of continuous lidar data: Macrophysical, optical, and thermodynamic properties, *J. Geophys. Res.-Atmos.*, 113 (D20), <https://doi.org/10.1029/2007JD009680>, 2008.
- Campbell, J.R., S. Lolli, J.R. Lewis, Y. Gu, and E.J. Welton: Daytime Cirrus Cloud Top-of-Atmosphere Radiative Forcing Properties at a Midlatitude Site and their Global Consequence, *J. Appl. Meteorol. Clim.*, 5, 1667-1679, <https://doi.org/10.1175/JAMC-D-15-0217.1>, 2016.
- 575 Campbell, J. R., Dolinar, E. K., Lolli, S., Fochesatto, G. J., Gu, Y., Lewis, J. R., Marquis, J. W., McHardy, T. M., Ryglicki, R. R., and Welton, E. J.: Cirrus cloud top-of-the-atmosphere net daytime forcing in the Alaskan subarctic from ground-based MPLNET monitoring, *J. Appl. Meteor. and Climatol.*, 60 (1), 51-63, <https://doi.org/10.1175/JAMC-D-20-0077.1>, 2021.
- 580 Córdoba-Jabonero, C., Guerrero-Rascado, J. L., Toledo, D., Parrondo, M., Yela, M., Gil, M. and Ochoa, H. A.: Depolarization ratio of polar stratospheric clouds in coastal Antarctica: comparison analysis between ground-based Micro Pulse Lidar and space-borne CALIOP observations, *Atmos., Meas. Tech.*, 6 (3), 703-717, <https://doi.org/10.5194/amt-6-703-2013>, 2013.
- Córdoba-Jabonero, C., Andrey-Andrés, J., Gómez, L., Adame, J. A., Sorribas, M., Navarro-Comas, M., Puertedura, O., Cuevas, E., and Gil-Ojeda, M.: Vertical mass impact and features of Saharan dust intrusions derived from ground-based remote sensing in synergy with airborne in-situ measurements, *Atmospheric Environment*, 142, 420-429, <http://dx.doi.org/10.1016/j.atmosenv.2016.08.003>, 2016.
- 585 Córdoba-Jabonero, C., Lopes, F. J. S., Landulfo, E., Cuevas, E., Ochoa, H. and Gil-Ojeda, M.: Diversity on subtropical and polar cirrus clouds properties as derived from both ground-based lidars and CALIPSO/CALIOP measurements, *Atmos. Res.*, 183, 151–165, <https://doi.org/10.1016/j.atmosres.2016.08.015>, 2017.
- 590 Córdoba-Jabonero, C., Sicard, M., Ansmann, A., del Águila, A. and Baars, H.: Separation of the optical and mass features of particle components in different aerosol mixtures by using POLIPHON retrievals in synergy with continuous polarized Micro-Pulse Lidar (P-MPL) measurements, *Atmos. Meas. Tech.*, 11 (8), 4775-4795, <https://doi.org/10.5194/amt-11-4775-2018>, 2018.
- 595 Córdoba-Jabonero, C., Sicard, M., del Águila, A., Jiménez, M. and Zorzano, M.-P.: Performance of a dust model to predict the vertical mass concentration of an extreme Saharan dust event in the Iberian Peninsula: Comparison with continuous, elastic, polarization-sensitive lidars, *Atmos. Environ.*, 214, 116828, <https://doi.org/10.1016/j.atmosenv.2019.116828>, 2019.
- 600 Córdoba-Jabonero, C., Gómez-Martín, L., del Águila, A., Vilaplana, J. M., López-Cayuela, M.A., and Zorzano, M.-P.: Cirrus-induced shortwave radiative effects depending on their optical and physical properties: Case studies using simulations and measurements, *Atmos. Res.*, 246, 105095, 2020.
- Córdoba-Jabonero, C., Sicard, M., López-Cayuela, M.-A., Ansmann, A., Comerón, A., Zorzano, M.-P., Rodríguez-Gómez, A., and Muñoz-Porcar, C.: Aerosol radiative impact during the summer 2019 heatwave produced partly by an inter-continental Saharan dust outbreak - Part 1: Short-wave dust direct radiative effect, *Atmos. Chem. Phys.*, 21, 6455–6479, <https://doi.org/10.5194/acp-21-6455-2021>, 2021.
- 605

- Engelmann, R., Kanitz, T., Baars, H., Heese, B., Althausen, D., Skupin, A., Wandinger, U., Komppula, M., Stachlewska, I. S., Amiridis, V., Marinou, E., Mattis, I., Linné, H. and Ansmann, A.: The automated multiwavelength Raman polarization and water-vapor lidar PollyXT: The neXT generation, *Atmos. Meas. Tech.*, 9, 1767-1784, <https://doi.org/10.5194/amt-9-1767-2016>, 2016.
- 610 Fernald, F. G.: Analysis of atmospheric lidar observations: some comments, *Appl. Opt.*, 23 (5), 652, <https://doi.org/10.1364/AO.23.000652>, 1984.
- Flynn, C. J., Mendoza, A., Zheng, Y. and Mathur, S.: Novel polarization-sensitive micropulse lidar measurement technique, *Opt. Express*, 15 (6), 2785-2790, <https://doi.org/10.1364/OE.15.002785>, 2007.
- Freudenthaler, V.: The telecover test: A quality assurance tool for the optical part of a lidar system, Boulder, Colorado, 2008.
- 615 Freudenthaler, V.: About the effects of polarising optics on lidar signals and the Delta 90 calibration, *Atmos. Meas. Tech.*, 9, 4181-4255, <https://doi.org/10.5194/amt-9-4181-2016>, 2016.
- Giannakaki, E., Kokkalis, P., Marinou, E., Bartsotas, N. S., Amiridis, V., Ansmann, A., and Komppula, M.: The potential of elastic and polarization lidars to retrieve extinction profiles, *Atmos. Meas. Tech.*, 13, 893-905, <https://doi.org/10.5194/amt-13-893-2020>, 2020.
- 620 Gimmestad, G. G.: Reexamination of depolarization in lidar measurements, *Appl. Opt.*, 47 (21), 3795-3802, 2008.
- Groß, S., Esselborn, M., Weinzierl, B., Wirth, M., Fix, A. and Petzold, A.: Aerosol classification by airborne high spectral resolution lidar observations, *Atmos. Chem. Phys.*, 12 (10), 25983-26028, <https://doi.org/10.5194/acpd-12-25983-2012>, 2013.
- 625 Guerrero-Rascado, J. L., Costa, M. J, Bortoli, D., Silva, A. M., Lyamani, H., and Alados-Arboledas L: Infrared lidar overlap function: an experimental determination, *Opt. Express*, 18, 20350-20369, 2010.
- Jiménez, C., Ansmann, A., Donovan, D., Engelmann, R., Schmidt, J. and Wandinger, U.: Comparison between two lidar methods to retrieve microphysical properties of liquid-water clouds, *EPJ Web Conf.*, 176, 01032, <https://doi.org/10.1051/epjconf/201817601032>, 2018.
- 630 Jiménez, C., Ansmann, A., Engelmann, R., Haerig, M., Schmidt, J. and Wandinger, U.: Polarization lidar: an extended three-signal calibration approach, *Atmos. Meas. Tech.*, 12 (2), 1077-1093, <https://doi.org/10.5194/amt-12-1077-2019>, 2019.
- Klett, J. D.: Lidar inversion with variable backscatter/extinction ratios, *Appl. Opt.*, AO, 24 (11), 1638-1643, <https://doi.org/10.1364/AO.24.001638>, 1985.
- 635 Lewis, J. R., Welton, E. J., Molod, A. M. and Joseph, E.: Improved boundary layer depth retrievals from MPLNET, *J. Geophys. Res.-Atmos.*, 118 (17), 9870-9879, <https://doi.org/10.1002/jgrd.50570>, 2013.
- Lewis, J. R., Campbell, J. R., Welton, E. J., Stewart, S. A. and Haftings, P. C.: Overview of MPLNET Version 3 Cloud Detection, *J. Atmos. Oceanic Technol.*, 33 (10), 2113-2134, <https://doi.org/10.1175/JTECH-D-15-0190.1>, 2016.
- 640 Lolli, S., J.R. Campbell, J. Lewis, Y. Gu, J. Marquis, B-N. Chew, S-C. Liew, S. Salinas, and E.J. Welton: Daytime Top-of-the-Atmosphere Cirrus Cloud Radiative Forcing Properties at Singapore, *J. Appl. Meteor. Climatol.*, 56 (5), 1249-1257, <https://doi.org/10.1175/JAMC-D-16-0262.1>, 2017.
- Lolli, S., L.P. D'Adderio, J.R. Campbell, M. Sicard, E.J. Welton, A. Binci, A. Rea, A. Tokay, A. Comeron, 645 R. Barragan, J.M. Baldasano, S. Gonzalez, J. Bech, N. Afflitto, J.R. Lewis, and F. Madonna: Vertically

- Resolved Precipitation Intensity Retrieved through a Synergy between the Ground-Based NASA MPLNET Lidar Network Measurements, Surface Disdrometer Datasets and an Analytical Model Solution, *Remote Sens.*, 10, 1102; <https://doi.org/10.3390/rs10071102>, 2018.
- 650 Lolli, S., Vivone, G., Lewis, J. R., Sicard, M., Welton, E. J., Campbell, J. R., Comerón, A., D'Adderio, I. P., Tokay, A., Giunta, A., and Pappalardo, G.: Overview of the New Version 3 NASA Micro-Pulse Lidar Network (MPLNET) Automatic Precipitation Detection Algorithm, *Remote Sensing*, 12 (1), 71, <https://doi.org/10.3390/rs12010071>, 2020.
- 655 Mamouri, R.-E. and Ansmann, A.: Potential of polarization lidar to provide profiles of CCN- and INP-relevant aerosol parameters, *Atmos. Chem. Phys.*, 16 (9), 5905-5931, <https://doi.org/10.5194/acp-16-5905-2016>, 2016.
- Mamouri, R.-E. and Ansmann, A.: Potential of polarization/Raman lidar to separate fine dust, coarse dust, maritime, and anthropogenic aerosol profiles, *Atmos. Meas. Tech.*, 10 (9), 3403-3427, <https://doi.org/10.5194/amt-10-3403-2017>, 2017.
- 660 Marengo, F., V. Santacesaria, A. F. Bais, D. Balis, A. di Sarra, A. Papayannis, and C. Zerefos: Optical properties of tropospheric aerosols determined by lidar and spectrophotometric measurements (Photochemical Activity and Solar Ultraviolet Radiation campaign), *Appl. Opt.*, 36, 6875-6886, 1997.
- Mattis, I., Müller, D., Ansmann, A., Wandinger, U., Preißler, J., Seifert, P. and Tesche, M.: Ten years of multiwavelength Raman lidar observations of free-tropospheric aerosol layers over central Europe: Geometrical properties and annual cycle, *J. Geophys. Res.-Atmos.*, 113, D20202, <https://doi.org/10.1029/2007JD009636>, 2008.
- 665 Mishchenko, M. I., and J. W. Hovenier: Depolarization of light backscattered by randomly oriented nonspherical particles, *Opt. Lett.*, 20 (12), 1356-1358, 1995.
- Pappalardo, G., Amodeo, A., Pandolfi, M., Wandinger, U., Ansmann, A., Bösenberg, J., Matthias, V., Amiridis, V., Tomasi, F. D., Frioud, M., Iarlori, M., Komguem, L., Papayannis, A., Rocadenbosch, F. and Wang, X.: Aerosol lidar intercomparison in the framework of the EARLINET project. 3. Raman lidar algorithm for aerosol extinction, backscatter, and lidar ratio, *Appl. Opt.*, AO, 43 (28), 5370-5385, <https://doi.org/10.1364/AO.43.005370>, 2004.
- 670 Pappalardo, G., Mona, L., D'Amico, G., Wandinger, U., Adam, M., Amodeo, A., Ansmann, A., Apituley, A., Arboledas, L. A., Balis, D., Boselli, A., Bravo-Aranda, J. A., Chaikovsky, A., Comeron, A., Cuesta, J., De Tomasi, F., Freudenthaler, V., Gausa, M., Giannakaki, E., Giehl, H., Giunta, A., Grigorov, I., Gross, S., Haefelin, M., Hiebsch, A., Iarlori, M., Lange, D., Linne, H., Madonna, F., Mattis, I., Mamouri, R. E., McAuliffe, M. A. P., Mitev, V., Molero, F., Navas-Guzman, F., Nicolae, D., Papayannis, A., Perrone, M. R., Pietras, C., Pietruczuk, A., Pisani, G., Preissler, J., Pujadas, M., Rizi, V., Ruth, A. A., Schmidt, J., Schnell, F., Seifert, P., Serikov, I., Sicard, M., Simeonov, V., Spinelli, N., Stebel, K., Tesche, M., Trickl, T., Wang, X., Wagner, F., Wiegner, M., Wilson, K. M.: Four-dimensional distribution of the 2010 Eyjafjallajökull volcanic cloud over Europe observed by EARLINET, *Atmos. Chem. Phys.*, 13, 4429-4450, <https://doi.org/10.5194/acp-13-4429-2013>, 2013.
- 680 Pappalardo, G., Amodeo, A., Apituley, A., Comeron, A., Freudenthaler, V., Linné, H., Ansmann, A., Bösenberg, J., D'Amico, G., Mattis, I., Mona, L., Wandinger, U., Amiridis, V., Alados-Arboledas, L.,

- 685 Nicolae, D. and Wiegner, M.: EARLINET: towards an advanced sustainable European aerosol lidar network, *Atmos. Meas. Tech.*, 7 (8), 2389-2409, <https://doi.org/10.5194/amt-7-2389-2014>, 2014.
- Sassen, K.: Lidar: range-resolved optical remote sensing of the atmosphere, chap. Polarization in lidar, no. 2 in *Springer Series in Optical Sciences*, Springer Science+ Business Media Inc., Springer-Verlag, New York., 2005.
- 690 Schmidt, J., Wandinger, U. and Malinka, A.: Dual-field-of-view Raman lidar measurements for the retrieval of cloud microphysical properties, *Appl. Opt.*, AO, 52 (11), 2235-2247, <https://doi.org/10.1364/AO.52.002235>, 2013.
- Sicard, M., Izquierdo Miguel, R., Alarcón Jordán, M., Belmonte Soler, J., Comerón Tejero, A. and Baldasano Recio, J. M.: Near-surface and columnar measurements with a micro pulse lidar of atmospheric pollen in Barcelona, Spain, *Atmos. Chem. Phys.*, 16 (11), 6805-6821, <https://doi.org/10.5194/acp-16-6805-2016>, 2016.
- 695 Sicard, M., Rodríguez-Gómez, A., Comerón, A., Muñoz-Porcar, C.: Calculation of the Overlap Function and Associated Error of an Elastic Lidar or a Ceilometer: Cross-Comparison with a Cooperative Overlap-Corrected System, *Sensors*, 20 (21), 6312, <https://doi.org/10.3390/s20216312>, 2020.
- 700 Sicard, M., Córdoba-Jabonero, C., López-Cayuela, M.-Á., Ansmann, A., Comerón, A., Zorzano, M.-P., Rodríguez-Gómez, A., and Muñoz-Porcar, C.: Aerosol radiative impact during the summer 2019 heatwave produced partly by an inter-continental Saharan dust outbreak – Part 2: Long-wave and net dust direct radiative effect, *Atmos. Chem. Phys.*, (in revision), 2021.
- Sigma Space Corporation, Micro-Pulse Lidar system information handbook, 2018.
- 705 Sugimoto, N., Matsui, I., Shimizu, A. and Nishizawa, T.: Lidar Network for Monitoring Asian Dust and Air Pollution Aerosols, in *IGARSS 2008 - 2008 IEEE International Geoscience and Remote Sensing Symposium*, vol. 2, p. II-573-II-576., 2008.
- Tesche, M., A. Ansmann, D. Müller, D. Althausen, R. Engelmann, V. Freudenthaler, and S. Groß: Vertically resolved separation of dust and smoke over Cape Verde using multiwavelength Raman and polarization lidars during Saharan Mineral Dust Experiment 2008, *J. Geophys. Res.*, 114, D13202, <https://doi.org/10.1029/2009JD011862>, 2009.
- 710 Tesche, M., S. Gross, A. Ansmann, D. Müller, D. Althausen, V. Freudenthaler and M. Esselborn: Profiling of Saharan dust and biomass-burning smoke with multiwavelength polarization Raman lidar at Cape Verde, *Tellus B: Chemical and Physical Meteorology*, 63:4, 649-676, <https://doi.org/10.1111/j.1600-0889.2011.00548.x>, 2011.
- 715 Toledo, D., Córdoba-Jabonero, C., and Gil, M.: Cluster Analysis: A New Approach Applied to Lidar Measurements for Atmospheric Boundary Layer Height Estimation, *J. Atmos. Ocean. Techn.*, 31, 422-436, <https://doi.org/10.1175/JTECH-D-12-00253.1>, 2014.
- Toledo, D., Córdoba-Jabonero, C., Adame, J. A., de la Morena, B., Gil-Ojeda, M.: Estimation of the atmospheric boundary layer height during different atmospheric conditions: a comparison on reliability of several methods applied to lidar measurements, *Int. J. Rem. Sens.*, 38:11, 3203-3218, <https://doi.org/10.1080/01431161.2017.1292068J>, 2017.
- 720 Wandinger, U. and Ansmann, A.: Experimental determination of the lidar overlap profile with Raman lidar, *Appl. Opt.*, AO, 41 (3), 511-514, <https://doi.org/10.1364/AO.41.000511>, 2002.

- 725 Wandinger, U., Freudenthaler, V., Baars, H., Amodeo, A., Engelmann, R., Mattis, I., Groß, S., Pappalardo, G., Giunta, A., D'Amico, G., Chaikovsky, A., Osipenko, F., Slesar, A., Nicolae, D., Belegante, L., Talianu, C., Serikov, I., Linné, H., Jansen, F., Apituley, A., Wilson, K. M., de Graaf, M., Trickl, T., Giehl, H., Adam, M., Comerón, A., Muñoz-Porcar, C., Rocadenbosch, F., Sicard, M., Tomás, S., Lange, D., Kumar, D., Pujadas, M., Molero, F., Fernández, A. J., Alados-Arboledas, L., Bravo-Aranda, J. A., Navas-Guzmán, F.,
- 730 Guerrero-Rascado, J. L., Granados-Muñoz, M. J., Preißler, J., Wagner, F., Gausa, M., Grigorov, I., Stoyanov, D., Iarlori, M., Rizi, V., Spinelli, N., Boselli, A., Wang, X., Lo Feudo, T., Perrone, M. R., De Tomasi, F. and Burlizzi, P.: EARLINET instrument intercomparison campaigns: overview on strategy and results, *Atmos. Meas. Tech.*, 9 (3), 1001-1023, <https://doi.org/10.5194/amt-9-1001-2016>, 2016.
- 735 Welton, E. J., Campbell, J. R., Spinhirne, J. D. and Scott III, V. S.: Global monitoring of clouds and aerosols using a network of micropulse lidar systems, in *Lidar Remote Sensing for Industry and Environment Monitoring*, vol. 4153, pp. 151–158, International Society for Optics and Photonics., 2001.
- Welton, E. J. and Campbell, J. R.: Micropulse Lidar Signals: Uncertainty Analysis, *J. Atmos. Oceanic Technol.*, 19 (12), 2089-2094, [https://doi.org/10.1175/1520-0426\(2002\)019<2089:MLSUA>2.0.CO;2](https://doi.org/10.1175/1520-0426(2002)019<2089:MLSUA>2.0.CO;2), 2002.
- 740 Welton, E. J., Stewart, S. A., Lewis, J. R., Belcher, L. R., Campbell, J. R., and Lolli, S.: Status of the Micro Pulse Lidar Network (MPLNET): Overview of the network and future plans, new version 3 data products, and the polarized MPL, *EPJ Web Conf.*, 176, 09003, <https://doi.org/10.1051/epjconf/201817609003>, 2018.
- Yu, H., Chin, M., Bian, H., Yuan, T., Prospero, J. M., Omar, A. H., Remer, L. A., Winker, D. M., Yang, Y., Zhang, Y. and Zhang, Z.: Quantification of trans-Atlantic dust transport from seven-year (2007–2013) record of CALIPSO lidar measurements, *Remote Sens. Environ.*, 159, 232-249, <https://doi.org/10.1016/j.rse.2014.12.010>, 2015.